

The Tropical Pacific ENSO–Mean State Relationship in Climate Models over the Last Millennium

D. ALLIE WYMAN

Department of Geology, University of Illinois at Urbana–Champaign, Urbana, Illinois

JESSICA. L. CONROY

Department of Geology, and Department of Plant Biology, University of Illinois at Urbana–Champaign, Urbana, Illinois

CHRISTINA KARAMPERIDOU

Department of Atmospheric Sciences, University of Hawai'i at Mānoa, Honolulu, Hawaii

(Manuscript received 11 September 2019, in final form 28 May 2020)

ABSTRACT


ENSO and the mean zonal sea surface temperature gradient (dSST) of the tropical Pacific are important drivers of global climate and vary on decadal to centennial time scales. However, the relationship between dSST and ENSO cannot be assessed with the short instrumental record, and is uncertain in proxy data, with intervals of both stronger and weaker ENSO postulated to occur with overall strong dSST in the past. Here we assess the ENSO–dSST relationship during the last millennium using general circulation models (GCMs) participating in phase 3 of the Paleoclimate Modeling Intercomparison Project. Last millennium GCM simulations show diversity in the strength and direction of the ENSO–dSST relationship. Yet, the models that best simulate modern tropical Pacific climate frequently have a more negative ENSO–dSST correlation. Thus, last millennium tropical Pacific climate simulations support the likelihood of enhanced ENSO during decadal to centennial periods of reduced tropical Pacific dSST. However, the alternating directional ENSO–dSST relationship in all model simulations suggests that this relationship is not constant through time and is likely controlled by multiple mechanisms.


1. Introduction

ENSO strength is known to vary on multidecadal to centennial time scales (Cobb et al. 2013, 2003; Deser et al. 2012; Karamperidou et al. 2014; Wittenberg 2009) and is hypothesized to be related to the mean state, or background conditions, of the tropical Pacific (Collins et al. 2010; Conroy et al. 2010; Fedorov and Philander 2001; Ford et al. 2015; Koutavas and Joanides 2012; Rustic et al. 2015; Sadekov et al. 2013). This relationship has implications for both forecasting ENSO and

projecting ENSO changes with anthropogenic forcing, but the instrumental record remains too short to adequately assess the nature of the ENSO–mean state relationship. Paleoclimate data offer a means to examine the ENSO–mean state relationship on longer time scales, yet sparse data with limited temporal resolution continue to hinder understanding of the direction and stationarity of this relationship in the past. For example, some recent studies conclude ENSO was stronger in the past with a stronger tropical Pacific zonal SST gradient, a common mean state metric (Ford et al. 2015), whereas others conclude ENSO was stronger in the past with a weaker zonal SST gradient (Koutavas and Joanides 2012; Rustic et al. 2015; Sadekov et al. 2013). Another assessment suggests the possibility of no relationship, or no consistent relationship, through time between ENSO variance and the zonal SST gradient (Conroy et al. 2010).

Apart from differences in the hypothesized direction of the ENSO–mean state relationship in the past, the mechanisms invoked to explain this relationship—rooted

 Denotes content that is immediately available upon publication as open access.

 Supplemental information related to this paper is available at the Journals Online website: <https://doi.org/10.1175/JCLI-D-19-0673.s1>.

Corresponding author: Allie Wyman, dawyman2@illinois.edu

DOI: 10.1175/JCLI-D-19-0673.1

© 2020 American Meteorological Society. For information regarding reuse of this content and general copyright information, consult the [AMS Copyright Policy](#) (www.ametsoc.org/PUBSReuseLicenses).

in modern observations and modeling—also vary. Frequently, the mean state, which varies due to both internal and external forcing, is considered as the driver of past changes in ENSO variance (Fedorov and Philander 2001). Several studies have explored the sensitivity of ENSO to changes in the mean state using models of varying complexity. These studies identified various parameters including zonal SST gradient strength, thermocline depth in the eastern Pacific, the strength of the equatorial upwelling, and surface wind intensity to be among key drivers of ENSO variability (Battisti and Hirst 1989; Dewitte 2000; Wittenberg 2002; Zebiak and Cane 1987). Further studies have explored ENSO variability during time periods with different radiative forcings and background conditions. For example, early Holocene ENSO variance was shown to be reduced due to cooler mean state SST, a weaker thermocline, and weakened horizontal currents (Roberts et al. 2014). Additionally, mid-Holocene orbital forcing of the distribution of seasonal insolation, in combination with upwelling in the eastern Pacific, is thought to have enhanced the zonal SST gradient across the Pacific. This enhanced gradient may have inhibited the development of El Niño events and reduced ENSO variance (Clement et al. 2000; Masson-Delmotte et al. 2013). Both long-term and short-term changes in subsurface temperatures and thermocline structure may have also altered ENSO variance by changing the balance of the many associated feedbacks that control ENSO (Ford et al. 2015; Karamperidou et al. 2015; Timmermann 2003). A stronger mean zonal SST gradient can also lead to an increase in the ENSO maximum potential intensity, thus increasing the frequency of stronger ENSO events (An and Jin 2004). Additionally, mean state SST anomalies can influence critical atmospheric ENSO feedbacks and key ENSO properties like skewness and seasonal phase locking (Bayr et al. 2018). Model biases in tropical Pacific mean state SST are thus likely key contributors to the ENSO biases observed in models through their role in influencing these feedbacks (Bayr et al. 2018; Bellenger et al. 2014; Ferrett et al. 2018).

However, ENSO may also influence the mean state. Nonlinear ENSO rectification on the mean state suggests that the known asymmetry between El Niño and La Niña events (with stronger El Niño vs La Niña events) causes residual heat from El Niño events to continue warming the eastern Pacific cold tongue long after an event ends (An and Jin 2004; Dewitte et al. 2009; Hayashi and Jin 2017; Jin et al. 2003; Liang et al. 2012; Sun 2003; Timmermann 2003; Timmermann and Jin 2002; Yeh and Kirtman 2004). The net effect of rectification is a multidecadal weakening of the zonal SST gradient as a result of strong El Niño events. Another

hypothesis also invokes ENSO asymmetry to explain a weaker zonal SST gradient coincident with enhanced ENSO variability, through recharge and loss of upper-ocean heat content in the western equatorial Pacific during ENSO events (Karnauskas et al. 2012). The reddening of high-frequency noise, due to the thermal inertia of the ocean, may also be the link between ENSO and mean state properties (Samanta et al. 2018). While these are certainly not the only means by which ENSO influences the tropical Pacific mean state, they do highlight ENSO's role in altering the mean state, and have been considered in explanations of the direction of the ENSO–mean state relationship in the past (Koutavas and Joanides 2012; Rustic et al. 2015; Sadekov et al. 2013). Indeed, model biases in the simulation of ENSO feedbacks have been linked to potential biases in the mean warming patterns of tropical Pacific SST in future climate scenarios (Karamperidou et al. 2017), illustrating that the relationship between the tropical Pacific mean state and ENSO variability is interactive and complex.

Last millennium transient simulations that include natural forcing factors are an ideal medium in which to address the question of the directionality of the ENSO–mean state relationship in the absence of large, externally forced background climate changes. The last millennium is a time period with similar background forcing to the twentieth century, prior to the advent of anthropogenic forcing, and thus adequately captures natural variability in the modern climate system. Annually resolved paleo-ENSO data are also most abundant during this time interval, permitting limited data–model comparisons. Phase 3 of the Paleoclimate Modeling Intercomparison Project (PMIP3) provides a means to comprehensively assess the last millennium ENSO–mean state relationship within many different models with the same imposed radiative forcing (Braconnot et al. 2012).

Climate model simulations can also be used to explore the assumption of stationarity, in this case the unidirectionality implicit in many discussions of the past ENSO–mean state relationship. Limited inquiries into whether the directionality of this relationship varies over time have been carried out, due to the scarcity of high-resolution paleo-ENSO data. GCM simulations provide an additional avenue for assessing ENSO–mean state interactions in models, and have the temporal resolution and length (i.e., at least 300–500 years) to address the question of stationarity (Karnauskas et al. 2012; Wittenberg 2009). Here we examine a suite of PMIP3 last millennium and preindustrial control simulations to assess the ENSO–mean state relationship on multi-decadal to centennial time scales. We seek to address the directionality of the ENSO–mean state relationship over the last millennium, the degree of model–proxy

TABLE 1. PMIP3/CMIP5 climate model information for this study. All past1000 simulations extend from 850 to 1850 CE. An asterisk indicates that three different experiments with different volcanic forcings were considered. P124 uses the [Crowley et al. \(2008\)](#) dataset, P126 has no volcanic forcing, and P128 uses [Gao et al. \(2008\)](#) dataset.

Organization	Model	Experiments
National Center for Atmospheric Research	CCSM4	piControl, past1000
University of New South Wales, Australia	CSIRO Mk3L-1.2	piControl, past1000
Met Office Hadley Centre	HadCM3	piControl, past1000
Institut Pierre-Simon Laplace	IPSL-CM5A-LR	piControl, past1000
Max Planck Institute for Meteorology	MPI-ESM-P	piControl, past1000
Meteorological Research Institute	MRI-CGCM3	piControl, past1000
National Aeronautics and Space Administration	GISS-E2-R	piControl, past1000: P124, P126, and P128*

agreement, and whether the relationship has remained stationary through time. This paper is organized as follows: the simulations used in this study, along with analytical methods, are presented in [section 2](#). [Section 3](#) presents the results of the modeling analysis and [section 4](#) discusses the last millennium ENSO–mean state relationship in models, reviews the state of understanding of this relationship from the available proxy data, and addresses implications for future ENSO variability. The paper concludes with a summary in [section 5](#).

2. Methods

Seven GCMs participating in both the last millennium (past1000) and preindustrial control (piControl) experiments of PMIP3, part of phase 5 of the Coupled Model Intercomparison Project (CMIP5), were used to assess the relationship between the zonal gradient of tropical Pacific SST (dSST) and ENSO variability ([Table 1](#)). All piControl simulations used in this analysis approximate conditions at 1850 CE. Each model’s piControl simulation was assessed using ENSO metrics ([section 2a](#)) relative to observational data to determine model skill in simulating ENSO. Similarly, each model’s piControl simulation was also assessed using mean state metrics ([section 2b](#)) to determine model skill in simulating the mean state. The GISS-E2-R piControl experiment includes four simulations with varying forcing factors. In this study, we use the GISS-E2-R P1 simulation as it is the longest of the four simulations (550 years). We disregard MIROC-ESM due to long-term drift in its past 1000 simulation.

Each past1000 simulation spans 850–1850 CE, and is forced with evolving boundary conditions, including volcanic and solar forcing, orbital variations, land use, and trace gases ([Schmidt et al. 2011, 2012](#)). The GISS-E2-R last millennium simulations assessed include three of eight different ensemble members: P124, P126, and P128. These ensemble members have different volcanic

forcing (P124: [Crowley et al. 2008](#); P126: none; P128: [Gao et al. 2008](#)) but the same solar, land use, greenhouse gas, and orbital forcing. These ensemble members were chosen because, while not exactly the same, their boundary conditions are most similar to those for the GISS-E2-R piControl simulation, facilitating a more direct comparison.

a. ENSO metrics

Metrics for ENSO variability (amplitude; [Bellenger et al. 2014](#)), and ENSO asymmetry (skewness) were calculated using Niño-3 (5°N–5°S, 150°–90°W) monthly SST anomalies. Amplitude and skewness were determined from the overall standard deviation and skewness of the Niño-3 monthly SST anomalies, respectively. Alpha, an ENSO nonlinearity metric that is the leading coefficient of the quadratic curve fit of the first two principal components of tropical Pacific SST anomalies, was determined as described in [Karamperidou et al. \(2017\)](#). This metric was shown to reflect the relative balance of ENSO feedbacks that leads to the presence of ENSO diversity (or ENSO “flavors”; i.e., strong eastern Pacific and moderate central Pacific events). The model metrics were compared to the same metrics calculated from HadISST1.1 monthly observations ([Rayner et al. 2003](#)) from 1870 to 2017. Similarity to the observations was assessed using

Normalized metric

$$= \frac{|\text{Model metric value} - \text{Observation metric value}|}{\text{Intermodel metric standard deviation}},$$

as per [Bellenger et al. \(2014\)](#). Lower numbers indicate higher degree of similarity to the observations ([Fig. 1](#), [Fig. S1](#) in the online supplemental material).

b. Mean state metrics

Metrics for mean state bias (R), multidecadal dSST variability (power), and SST magnitude [mean bias error (MBE)] were used to determine model skill in

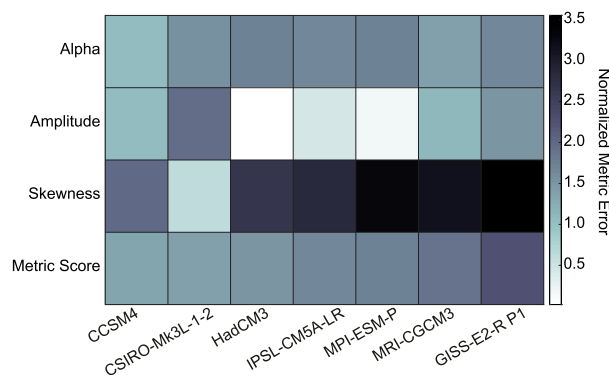


FIG. 1. ENSO metrics calculated with preindustrial control Niño-3 SST anomalies. The color bar is normalized error compared to observations (HadISST1.1). Light colors indicate strong agreement with observations; dark colors indicate weaker agreement. Observation alpha = 0.29, amplitude = 0.80, and skewness = 0.78. Models are listed in order of agreement with observations. Metric values can be found in Table S1.

simulating the mean state. Note that R is the pattern correlation coefficient between time-averaged model and observational (HadISST1.1) equatorial Pacific SST (5°N–5°S, 150°E–80°W). Power in both models and observations was determined using the 8–20 year average of the dSST power spectrum. The power spectra were calculated using the WaveletComp package in the statistical software R, which applies the Morlet wavelet to a dataset. dSST is defined as western equatorial Pacific SST (5°N–5°S, 100°E–180°) subtracted by eastern equatorial Pacific SST (5°N–5°S, 160°–80°W). MBE is the mean bias error between time-averaged, detrended, observational SST and time-averaged, model SST across the equator. HadISST was detrended to remove any anthropogenic warming trend in modern SST prior to comparison with models. Metric similarity to the observations was assessed using the normalized metric equation presented in section 2a. Lower numbers indicate higher degree of similarity to the observations (Fig. 2, Fig. S2). All analysis in future sections are conducted on average annual values and thus mean state seasonal metrics are not considered here.

c. Model ENSO–dSST assessment

The past1000 and piControl experiments for each model were used to assess the ENSO–dSST relationship. For each simulation, a dSST time series was created using SST data averaged from the same western equatorial Pacific and eastern equatorial Pacific regions defined in section 2b. Data were low-pass filtered to remove frequencies (<7 years) associated with ENSO. After filtering, the data were averaged to create an annual average dSST time series. Similarly, a Niño-3 time

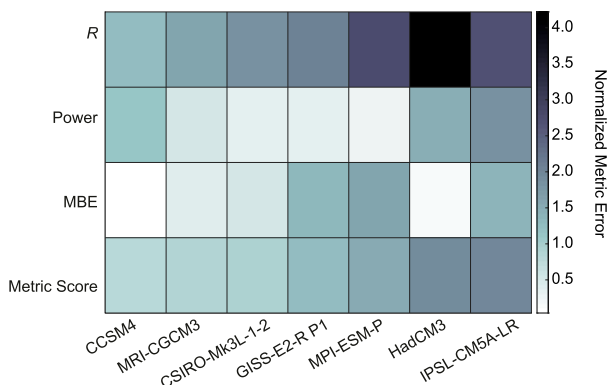


FIG. 2. Tropical Pacific mean state metrics calculated with preindustrial control SST data. The color bar is normalized error compared to observations (HadISST1.1). Light colors indicate strong agreement with observations; dark colors indicate weaker agreement. Observation $R = 1$, power = 0.22, and MBE = 0. Models are listed in order of agreement with observations. Metric values can be found in Table S1.

series was created from monthly Niño-3 anomalies, bandpass filtered with a 4-month to 7-yr window to remove low-frequency mean state variability while keeping frequencies associated with ENSO. After filtering, December–February (DJF) anomalies were averaged together to obtain an annual Niño-3 DJF anomaly time series.

To assess the multidecadal relationship between ENSO variability and dSST in past1000 and piControl model simulations, 40-yr moving standard deviations were calculated for Niño-3 and 40-yr moving averages were calculated for dSST. To assess the directionality of the mean state–ENSO variability relationship, 60-yr moving correlation coefficients were calculated between the Niño-3 standard deviation and mean dSST time series; 40-yr moving windows were chosen for a more direct comparison to proxy dSST records with a minimum 40-yr resolution (see the appendix). Various correlation windows (40, 50, 60, 70, 80, and 90 years) were tested and 60-yr correlations appeared representative for each model. Autocorrelation in each time series was calculated and used to determine the effective sample size (Dawdy and Matalas 1964) and statistical significance of the correlations.

Red noise testing of the ENSO–dSST relationship in past1000 models simulations was conducted as another means of determining significance. Using the autocorrelative parameters of the raw ENSO monthly anomalies, 10 000 time series with the autoregression [AR(1)] coefficient and mean of the original were created, then filtered, for each model. The same 40-yr running standard deviation was applied to the 10 000 time series. This process was repeated with raw model dSST to create 10 000 dSST red noise time series with

the same AR(1) coefficient and mean of the original for each model. These time series also underwent the same filtering and 40-yr averaging. We calculated 60-yr running correlations between dSST and ENSO for both ENSO and red noise dSST as well as red noise ENSO and dSST. Last, the red noise ENSO and red noise dSST were correlated together as well. Skewness was calculated on each distribution of model correlations and noise correlations to determine the symmetry of the distributions (see Fig. 4 below). Skewness of each distribution provided a metric to assess similarity between all noise correlations and model correlations.

3. Results

a. Climate model ENSO and mean state

Metrics of ENSO nonlinearity (alpha), ENSO variability (amplitude), and ENSO skewness, as compared to observational values, vary from model to model (Fig. 1). The GCMs with preindustrial control ENSO metrics that most closely approximate observations for each category were CCSM4 (alpha), HadCM3 (amplitude), and CSIRO Mk3L (skewness). The GCMs with preindustrial control ENSO metrics furthest from observations were HadCM3 (alpha), CSIRO Mk3L (amplitude), and GISS-E2-R (skewness). Thus, no GCM was closest to or furthest from observations in more than one category (Table S1), necessitating the use of averaging scores across categories to determine the average metric error, a measure of the highest and lowest performing models. Overall, the highest performing GCMs were CCSM4 and CSIRO Mk3L and the lowest performing GCMs were MRI-CGCM3 and GISS-E2-R.

Model skill in simulating the mean state was assessed by correlating the pattern of simulated mean annual SST with observational SST across the equatorial Pacific (R), assessing multidecadal variability in dSST in models (power), and assessing differences in SST magnitude between models and observations (MBE; Fig. 2). Correlating model with observational SST patterns revealed correlations higher than 0.60 in most models, with the highest correlation in CCSM4. The lowest correlations were found in HadCM3. While CCSM4 also showed the most multidecadal variability of any model (Fig. S2), MPI-ESM-P and CSIRO Mk3L most closely matched observed multidecadal dSST power. IPSL-CM5A-LR had the least multidecadal variability of any GCM. The model most similar to observations in terms of SST magnitude was CCSM4 and the furthest from observations was MPI-ESM-P (Fig. 2, Fig. S3). The average of normalized scores revealed that the highest ranking GCMs were CCSM4 and MRI-CGCM3 and the

lowest ranking models were HadCM3 and IPSL-CM5A-LR (Table S1).

b. ENSO–dSST relationship over the last millennium

The ENSO–dSST relationship over the last millennium varies substantially between different GCM simulations. Time series of past1000 dSST and ENSO reveal no similarities in dSST or ENSO variability across models (Fig. 3). Additionally, time series of correlation coefficients representing the ENSO–dSST relationship are nonstationary, alternating between negative and positive correlations in all models. The distributions of these correlation coefficients in most models are moderately skewed ($0.5 < \text{skewness} < 1$), with primarily negative correlation coefficients (Fig. 4). Correlation distributions in CCSM4 and GISS-E2-R P126 are highly skewed ($\text{skewness} > 1$), with correlations that are overwhelmingly negative. Only two of the models assessed here, MRI-CGCM3 and GISS-E3-R P128, have correlation distributions that are approximately symmetric ($0 < \text{skewness} < 0.5$). While correlation distribution skewness does not neatly align with either overall dSST or ENSO rankings, it does appear that, generally speaking, skewness decreases as the average ranking (e.g., model performance) decreases (Table S1), with the exception of the GISS-E2-R models. Comparison of the model correlation distributions to correlations generated from red noise time series indicates the noise correlations are approximately symmetric for every model (s_1 – s_3 values, Fig. 4). Correlations between model metrics and ENSO–dSST correlation skewness shows the alpha and power metrics both have statistically significant ($p < 0.05$) correlations with last millennium ENSO–dSST correlation distribution skewness (Table S2).

To further explore the role of internal versus external forcing of the ENSO–mean state relationship, we compared past1000 and piControl ENSO–mean state correlation distribution skewness. The piControl correlation distributions are variable across models and there is no clear relationship with model skill in simulating ENSO and dSST (Fig. S4). CCSM4, GISS-E2-R, and HadCM3 piControl correlation distributions are moderately to highly positively skewed, similar to their past1000 counterparts. The remaining piControl correlation distributions are approximately symmetric, much like the noise distributions.

4. Discussion

We focus our discussion on the last millennium simulations in order to facilitate more direct comparison with last millennium proxy reconstructions of dSST and ENSO. In last millennium simulations, there is no

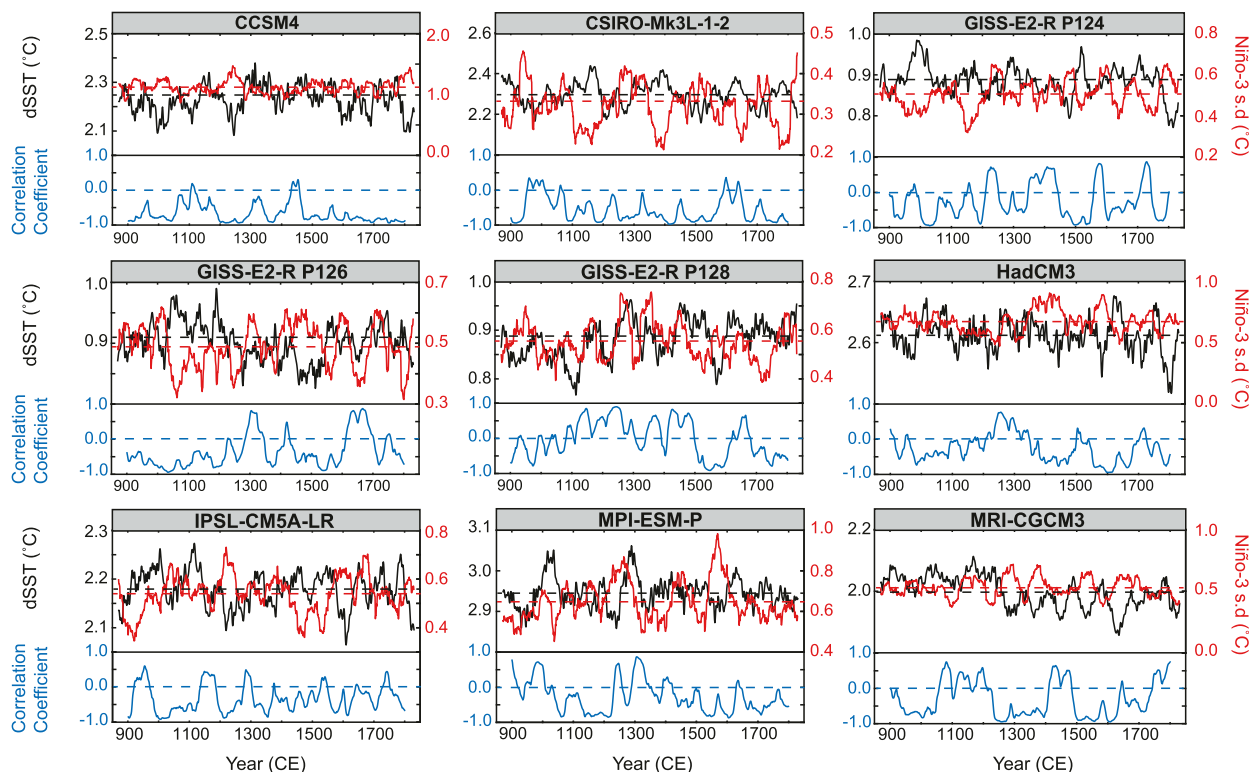


FIG. 3. Time series of 40-yr moving-average dSST (black), 40-yr moving ENSO standard deviation represented by Niño-3 (red), and 60-yr correlation coefficients (blue) of CMIP5 past1000 model simulations. Dashed black and red lines indicate the mean of dSST and ENSO, respectively. Dashed blue lines indicate a correlation coefficient of zero.

intermodel agreement in the magnitude or direction of dSST change or ENSO variability (Fig. 3), similar to control simulations (Fig. S5). However, there is a preponderance of negative correlations between multi-decadal dSST and ENSO variability in most models. The GCMs that more accurately simulate ENSO and the mean state show a more skewed distribution of correlations. These skewed distributions indicate the ENSO–mean state relationship is more frequently negative, with a stronger mean state (e.g., enhanced zonal gradient) co-occurring with reduced ENSO variability. Overall, correlation distribution skewness decreases as simulation skill decreases, with the exception of the GISS-E2-R models (Fig. 4).

The models showing similar piControl and past1000 correlation distribution patterns suggests internal variability is the primary driver of the ENSO–mean state relationship (Coats and Karneuskas 2017; Karneuskas et al. 2012; Wittenberg 2009). For some models, however, piControl distribution is not significantly different than the noise distributions, while the past1000 is positively skewed due the prevalence of more negative ENSO–dSST correlations. This suggests that external

forcing, most likely, volcanic forcing, shapes the ENSO–dSST relationship in these models. Climate models have a demonstrated ENSO sensitivity to volcanic eruptions with a recent study showing highly variable ENSO response to volcanic forcing in CMIP5/PMIP3 models (Dee et al. 2020; Pausata et al. 2016, 2020; Stevenson et al. 2016). The potential influence of volcanism on the modeled ENSO–mean state relationship is further highlighted by the GISS-E2-R models used in this study. GISS-E2-R P124, P126, and P128 all have large differences in their ENSO–mean state correlation distribution skewness. The only difference between the GISS-E2-R models is the volcanic forcing, with P126 having no volcanic forcing and P124 and P128 using different volcanic forcing datasets [see Crowley et al. (2008) and Gao et al. (2008), respectively]. In addition to using a different volcanic forcing dataset from P124, P128 was noted to have double the radiative forcing due to a conversion error when specifying the volcanic forcing (Schmidt et al. 2013). The correlation distribution skewness in the GISS-E2-R simulations decreases as volcanic forcing increases, suggesting a potential volcanic influence on the mean state–ENSO relationship.

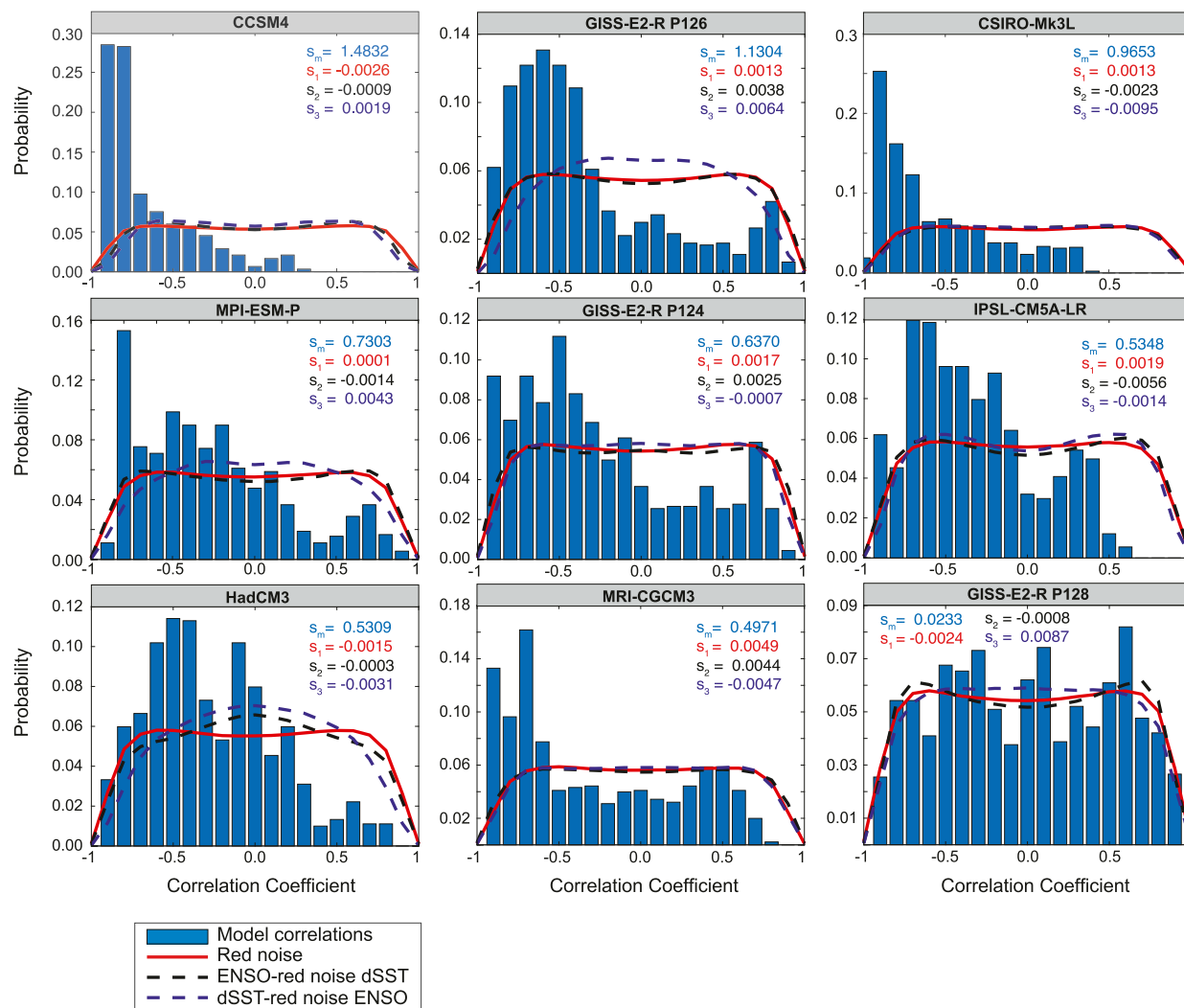


FIG. 4. Histograms of multidecadal past1000 dSST-ENSO correlation coefficients plotted against a series of red noise tests. Skewness values associated with model and each noise test are shown in each panel. Models are plotted in order from highest to lowest skewness starting from the upper-left corner and moving to the right.

This potential influence should be the subject of future research.

Paleoclimate data-model comparison is a valuable tool for both validating model output and understanding proxy climate data. However, limited paleoclimate data still preclude a thorough and conclusive assessment of the ENSO-mean state relationship, even in the last millennium, when data are most abundant. Monthly or annual ENSO reconstructions from corals are not continuous, and when statistically combined, interannual to decadal age model error can dampen ENSO variance estimates. Continuous, annual ENSO reconstructions from teleconnected regions are thus the only current means of adequately assessing ENSO variance in this time period but require the assumption of constant

ENSO teleconnections through time. For the mean state, continuous marine sediment based proxy SST records are relatively abundant in the western Pacific, but only one record, which is short in length and possibly prone to bioturbation, is currently available from the eastern Pacific. Nevertheless, here we conduct an initial exploration of the ENSO-dSST relationship in proxy records to demonstrate how this assessment can be done in the future when more records are available. We calculate a composite dSST record from 10 high-resolution proxy SST records and compare the resulting time series to the Li et al. (2011) Niño-3 reconstruction (hereafter Li), developed from the first principal component of the North American Drought Atlas (see the appendix). Similar to the model data, these datasets were compared in 40-yr

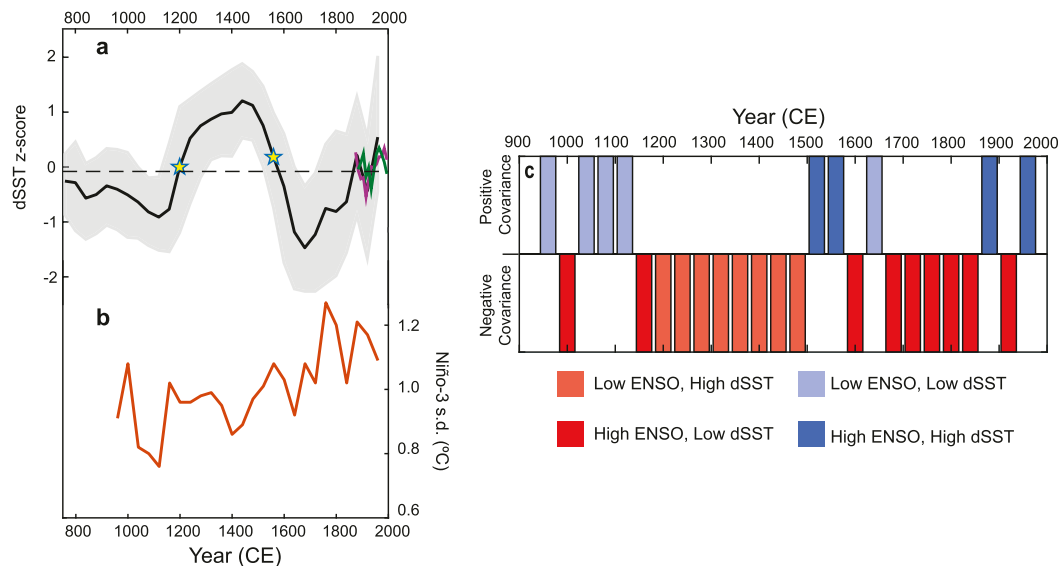


FIG. 5. ENSO and dSST information from paleoclimate observations. (a) dSST time series. The black line indicates the mean proxy dSST and the shading indicates the uncertainty. The dashed line indicates mean proxy dSST z score. The mean z score represents the west Pacific z score subtracted by the east Pacific z score resulting in a mean slightly below zero. Averaged dSST from ERSST (green) and HadISST (purple) are plotted in 10-yr intervals. (b) The 40-yr ENSO standard deviation of Li et al. (2011). (c) ENSO–dSST comparison between Li et al. (2011) and proxy dSST (see the appendix).

intervals. However, the proxy data resolution resulted in a low sample size, precluding the use of correlation coefficients in the analysis. Nonetheless, qualitative comparisons show a primarily negative relationship between ENSO and dSST, with some multidecadal periods of a positive relationship (Fig. 5b).

The negative and positive correlations observed in the models (and proxy data) suggest the assumption of a consistent ENSO–mean state relationship on multidecadal to centennial time scales, either in direction or strength, is not valid. However, the greater frequency of a negative relationship during the last millennium in models that best simulate ENSO and the mean state, as well as the available proxy data, suggests the hypothesized mechanisms that produce such a negative relationship on these time scales may be at work more frequently over the last millennium. These mechanisms include nonlinear ENSO rectification on the mean state, whereby a stronger ENSO reduces dSST, resulting in negative correlations. Or, the mean state may be the driver of ENSO strength, with a stronger zonal SST gradient inhibiting the development of El Niño events. Regardless, as the time periods of strong and weak, as well as negative and positive, ENSO–mean state relationships vary from model to model, the primary drivers of this relationship over the last millennium are likely variable, and internal in nature. However, differences in the degree of skewness between past1000 and piControl

experiments in some models (Fig. S4) suggests the ENSO–mean state relationship could also be partly influenced by external forcings on multidecadal to centennial time scales. This should be the subject of future research.

Historically, climate models have struggled to project ENSO variability that is consistent across models, with little to no intermodel consensus regarding future changes (Cai et al. 2015; Collins et al. 2010; Karamperidou et al. 2017; Meehl et al. 2007; Vecchi et al. 2008; Watanabe et al. 2011) unless models are subselected based on certain metrics (Cai et al. 2018; Karamperidou et al. 2017). Projected changes in the zonal SST gradient also conflict with modern observations. In this case, models show a weakening of the zonal SST gradient with increased greenhouse gas radiative forcing, but this trend has not been observed in twentieth-century SST datasets, and there is limited agreement between twentieth-century observations and simulations (Coats and Karnauskas 2017; DiNezio et al. 2013; Seager et al. 2019). The ultimate cause of this discrepancy is hypothesized to be model bias, in this case, a central-eastern Pacific equatorial cold tongue that is too cold (Seager et al. 2019) or too far west (Samanta et al. 2018) or biases in the simulation of the equatorial undercurrent (Coats and Karnauskas 2018). Simulations without a cold tongue bias show a strengthened zonal SST gradient, rather than a weakened gradient (Seager et al. 2019). Karamperidou et al. (2017) linked the

pattern of tropical Pacific SST change in future climate scenarios to model biases in simulating ENSO feedbacks and nonlinearity; they found that models with strong ENSO nonlinearity (alpha metric used here) tend to simulate less relative warming of the cold tongue compared to the entire equatorial Pacific, possibly due to their enhanced thermodynamic damping in the east Pacific. It may also be spuriously high variance in the western Pacific in models that produces centennial trends in dSST (Samanta et al. 2018). However, of the models assessed here, those with a cold tongue bias do not consistently have a more highly skewed or symmetric ENSO–dSST correlation distribution, suggesting that correcting for this cold tongue mean state bias may not inform on the future mean state–ENSO relationship. Additionally, the cold tongue bias was substantially improved in CMIP5 versus CMIP3 models, and yet, ENSO was not equally improved (Bellenger et al. 2014). Thus, an improved mean state does not necessarily imply improved ENSO. Furthermore, as our work shows, the mean state also cannot be used as a predictor of ENSO variability on multidecadal time scales, given the shifting direction and strength of this relationship. Further research into ENSO–mean state dynamics, particularly the oscillations between periods of positive and negative covariance between ENSO and the mean state, may elucidate mechanisms of tropical Pacific internal variability that further improve future projections of both ENSO and the mean state, either individually or in tandem.

5. Summary

The direction and stationarity of the ENSO–tropical Pacific mean state relationship is difficult to assess with the short observational record and remains uncertain in proxy data. However, this relationship has implications for the nature of both the future mean state and interannual variability in the tropical Pacific and teleconnected regions. The assessment presented here uses last millennium climate model simulations to determine the nature of the ENSO–dSST relationship on multidecadal to centennial time scales. Last millennium simulations from climate models with ENSO and dSST characteristics that best approximate observations show more frequent multidecadal periods of negative correlation coefficients between ENSO variability and dSST strength. The distributions of correlations are more symmetric in models that agree more poorly with observed ENSO and dSST statistics. Predominantly negative ENSO–dSST relationships are also seen in the available, but limited, proxy data. This relationship indicates increased ENSO strength frequently co-occurs with weaker dSST and vice versa during the last millennium. However, all model simulations and the proxy data also show alternating periods of positive and negative ENSO–dSST

relationships. Thus, the ENSO–dSST relationship is not unidirectional on these time scales, suggesting this relationship is dynamic. This observed alternating relationship and its underlying mechanisms should motivate future research as it will improve understanding of tropical Pacific internal variability and future climate projections of ENSO and the tropical Pacific mean state.

Acknowledgments. This work was funded by NSF AGS-1602580 and AGS-1602097 to C.K. and J.L.C. The authors thank Nick McKay for help with proxy age modeling, the Met Office and NOAA ERSST for providing observational SST data, CESM Earth System Grid for providing access to climate model data, and NOAA National Centers for Environmental Information for providing access to the proxy data used in this work. Last, the authors thank anonymous reviewers who helped improve this research. The authors declare no competing financial interests.

Data availability statement. NOAA ERSST V5 data were provided by the NOAA/OAR/ESRL PSD, Boulder, Colorado, from their website at <https://www.esrl.noaa.gov/psd/>. HadISST1.1 data are available on the Met Office Hadley Center website (<https://www.metoffice.gov.uk/hadobs/hadisst/>). CMIP5 data are available on the Earth System Grid Federation database (<https://esgf-node.llnl.gov/projects/cmip5/>). CESM data are available on the University Corporation for Atmospheric Research website (<http://www.cesm.ucar.edu/projects/community-projects/LME/data-sets.html>). All proxy data can be found in the supplemental information of the original publications or the NOAA Paleoclimatology database (<https://www.ncdc.noaa.gov/data-access/paleoclimatology-data>). All data that support the findings of this study are available as supplemental information.

APPENDIX

Proxy ENSO and dSST Assessment

a. Record selection

There are several estimates of dSST, and even more of ENSO variability, spanning parts of the last millennium. To compare last millennium ENSO–mean state relationships in the proxy and model data, we analyze, based on specific criteria, the most robust available estimates of both dSST and ENSO. For ENSO, these criteria are that the data are 1) continuous, 2) annually resolved, 3) have minimal age uncertainty, 4) span the last millennium, and 5) have been calibrated and verified with observations. The only ENSO dataset that meets these

criteria currently is Li. Li uses the first principal component of the North American Drought Atlas (NADA, version 2) developed from annually resolved North American tree-ring data to reconstruct Niño-3 variability. This ENSO reconstruction meets the above criteria, has a statistically robust relationship with Niño-3 SST, and is the longest (900–2002 CE) annually resolved reconstruction available to date. ENSO reconstructions that contain other types of annually resolved proxy data, mainly corals, were also considered, but the interannual to decadal chronology error on individual coral records can lead to incorrect estimates of past ENSO variability when they are combined. We acknowledge that because the Li reconstruction is based on terrestrial proxies and assumes a stationary hydroclimatic teleconnection with North America, there is also inherent uncertainty associated with using this reconstruction.

To assess changes in dSST through the last millennium, we combine proxy records from the western Pacific and eastern Pacific to create a composite dSST record from all available data. Proxy record criteria for selection included that each record 1) is marine; 2) contained quantitative planktonic foraminifera Mg/Ca or alkenone-based SST data; 3) had accessible age model data; 4) is continuous, with multidecadal resolution; and 5) is from within the eastern Pacific cold tongue (5°N–5°S, 120°–90°W), or western Pacific warm pool (10°N–10°S, 105°–135°E). These criteria allowed for the creation of the composite proxy dSST time series of the last millennium using only records that directly and quantitatively reconstruct SST (Fig. 5, Table S3). Of all existing paleoclimate records available for public use, nine records from the western Pacific and one from the eastern Pacific fit the above criteria (Fig. S6). Only one record from the western Pacific is alkenone based. As it is debated whether to mix alkenone and Mg/Ca estimates (Koutavas and Joanides 2012), we explored the impact of including this record in the estimate of dSST. Including this record (Zhaou et al. 2006) did not alter the dSST time series appreciably (Fig. S7).

b. Age uncertainty propagation in marine SST records

Inherent in every proxy record is some degree of age uncertainty. To combine each proxy record to create a dSST time series, the age uncertainty of each record was accounted for by creating 10 000 age–depth iterations of each paleoclimate record using the published age dates in Bchron. Bchron is a statistical package for generating age models from dated material (Haslett and Parnell 2008) using the reported ages, age uncertainty, sample

depth of dated material, and sample depths of nondated material to generate a suite of possible age models constrained by the uncertainty of the dated material. Using 10 000 possible age models for each record allows for a statistically robust examination of age uncertainty when combining said records. Allowing variations within age uncertainty produced some records that begin earlier or end later than published records, causing the composite dSST record to extend a bit further back in time than the originally published records.

c. Creating composite dSST record

All 10 000 iterations of each record were interpolated in 40-yr intervals between 760 and 1960 CE and normalized by subtracting the long-term mean and dividing by the standard deviation of each iteration. The interval 760–1960 CE was chosen as it spans the length of the newly modeled eastern Pacific record and western Pacific records and 40-yr intervals is the highest resolution allowable given the limits of individual proxy resolution. A composite western Pacific record was created by averaging each normalized record together. The normalized eastern Pacific record and composite western Pacific record are plotted in Fig. S8. The eastern Pacific time series was subtracted from the western Pacific time series to create 10 000 iterations of the dSST time series. These were sorted and the median time series was used for comparison to the Li ENSO time series. The 0.95 dSST quantile the 0.05 dSST quantile were used as bounds for age uncertainty. A z score above the mean for the sorted, median time series ($\mu_{\text{West}} = -0.07$, $\mu_{\text{East}} = 0.08$, $\mu_{\text{dSST}} = -0.15$) indicates above-average SST or dSST (°C). Regime shift detection on the proxy dSST time series was conducted per published methods in 120-yr windows (Rodionov 2004, 2006). Regime shift detection calculates the change in dSST needed for a shift to a new climate regime for each time step using the mean, variance, and test window length. ERSSTv5 (Huang et al. 2017) and HadISST1.1 SST data from the grids containing each proxy were also extracted and normalized to create western Pacific and eastern Pacific composite SST time series. These records were subtracted to produce the observed dSST record from 1880 to 2000, which is compared to the proxy dSST time series (Fig. 5a).

d. SST uncertainty propagation in marine proxy records

The published SST uncertainty for each proxy record ranges from 0.2° to 1.4°C and was normalized:

$$\text{Normalized uncertainty} = \frac{\text{SST uncertainty}}{\text{SST}},$$

where SST represents the interpolated SST for each time step in each record. The western Pacific uncertainties were combined:

$$\text{Uncertainty} = \frac{\left(\sqrt{\sum_{i=1}^n X_i^2} \right)}{n},$$

where X represents the uncertainty for a given record and n represents the number of records included. The east and west uncertainty was combined to obtain a total SST uncertainty for the proxy dSST time series:

$$\text{dSST Uncertainty} = \left(\sqrt{W^2 + E^2} \right),$$

where W represents the western Pacific uncertainty and E represents the eastern Pacific uncertainty. The combined uncertainty was added to the 0.95 dSST quantile and subtracted from the 0.05 dSST quantile in order to combine age uncertainty and SST uncertainty to create the most conservative estimate of uncertainty.

e. Proxy dSST–ENSO assessment

We calculated 40-yr standard deviations of the Li ENSO time series to assess multidecadal ENSO variability (Fig. 5). To assess the ENSO–dSST relationship on multidecadal time scales, ENSO reconstructions were also categorically compared to the proxy dSST time series over 40-yr windows (Fig. 5b). Such categorical assessments of paleoclimate data are a means to interpret paleoclimate data when limited sample size or the qualitative nature of the proxy interpretation precludes time series analysis (DiNezio and Tierney 2013; Higley et al. 2018; Oster et al. 2015). dSST and ENSO directionality was assessed by determining if dSST strength and ENSO variability were high or low over the time period. If dSST strength and ENSO variability were high or low at the same time, the two parameters were said to positively covary. If dSST was high while ENSO was low, or vice versa, they were said to negatively covary. ENSO variability was considered high if the analysis window standard deviation was higher than the standard deviation for the entire time series. dSST was considered high if the analysis window average was higher than the average for the entire time series.

REFERENCES

- An, S.-I., and F.-F. Jin, 2004: Nonlinearity and asymmetry of ENSO. *J. Climate*, **17**, 2399–2412, [https://doi.org/10.1175/1520-0442\(2004\)017<2399:NAAOE>2.0.CO;2](https://doi.org/10.1175/1520-0442(2004)017<2399:NAAOE>2.0.CO;2).
- Battisti, D. S., and A. C. Hirst, 1989: Interannual variability in a tropical atmosphere–ocean model: Influence of the basic state, ocean geometry, and nonlinearity. *J. Atmos. Sci.*, **46**, 1687–1712, [https://doi.org/10.1175/1520-0469\(1989\)046<1687:IVIATA>2.0.CO;2](https://doi.org/10.1175/1520-0469(1989)046<1687:IVIATA>2.0.CO;2).
- Bayr, T., M. Latif, D. Dommengot, C. Wengel, J. Harlaß, and W. Park, 2018: Mean-state dependence of ENSO atmospheric feedbacks in climate models. *Climate Dyn.*, **50**, 3171–3194, <https://doi.org/10.1007/s00382-017-3799-2>.
- Bellenger, H., E. Guilyardi, J. Leloup, M. Lengaigne, and J. Vialard, 2014: ENSO representation in climate models: From CMIP3 to CMIP5. *Climate Dyn.*, **42**, 1999–2018, <https://doi.org/10.1007/s00382-013-1783-z>.
- Braconnot, P., and Coauthors, 2012: Evaluation of climate models using palaeoclimatic data. *Nat. Climate Change*, **2**, 417–424, <https://doi.org/10.1038/nclimate1456>.
- Cai, W., and Coauthors, 2015: ENSO and greenhouse warming. *Nat. Climate Change*, **5**, 849–859, <https://doi.org/10.1038/nclimate2743>.
- , and Coauthors, 2018: Increased variability of eastern Pacific El Niño under greenhouse warming. *Nature*, **564**, 201–206, <https://doi.org/10.1038/s41586-018-0776-9>.
- Clement, A. C., R. Seager, and M. A. Cane, 2000: Suppression of El Niño during the mid-Holocene by changes in the Earth's orbit. *Paleoceanography*, **15**, 731–737, <https://doi.org/10.1029/1999PA000466>.
- Coats, S., and K. B. Karnauskas, 2017: Are simulated and observed twentieth century tropical Pacific sea surface temperature trends significant relative to internal variability? *Geophys. Res. Lett.*, **44**, 9928–9937, <https://doi.org/10.1002/2017GL074622>.
- , and —, 2018: A role for the equatorial undercurrent in the ocean dynamical thermostat. *J. Climate*, **31**, 6245–6261, <https://doi.org/10.1175/JCLI-D-17-0513.1>.
- Cobb, K. M., C. D. Charles, H. Cheng, and R. L. Edwards, 2003: El Niño/Southern Oscillation and tropical Pacific climate during the last millennium. *Nature*, **424**, 271–276, <https://doi.org/10.1038/nature01779>.
- , N. Westphal, H. R. Sayani, J. T. Watson, E. Di Lorenzo, H. Cheng, R. L. Edwards, and C. D. Charles, 2013: Highly variable El Niño–Southern Oscillation throughout the Holocene. *Science*, **339**, 67–70, <https://doi.org/10.1126/science.1228246>.
- Collins, M., and Coauthors, 2010: The impact of global warming on the tropical Pacific Ocean and El Niño. *Nat. Geosci.*, **3**, 391–397, <https://doi.org/10.1038/ngeo868>.
- Conroy, J., J. T. Overpeck, and J. E. Cole, 2010: El Niño/Southern Oscillation and changes in the zonal gradient of tropical Pacific sea surface temperature over the last 1.2 ka. *PAGES News*, **18**, 32–34, <https://doi.org/10.22498/PAGES.18.1.32>.
- Crowley, T. J., G. Zielinski, B. Vinther, R. Udisti, K. Kreutz, J. Cole-Dai, and E. Castellano, 2008: Volcanism and the Little Ice Age. *PAGES News*, **16**, 22–23, <https://doi.org/10.22498/pages.16.2.22>.
- Dawdy, D. R., and N. C. Matalas, 1964: Statistical and probability analysis of hydrologic data, part III: Analysis of variance, covariance and time series. *Handbook of Applied Hydrology, a Compendium of Water-Resources Technology*, V. T. Cho, Ed., McGraw-Hill Book Company, 68–90.
- Dee, S. G., K. M. Cobb, J. Emile-Geay, T. R. Ault, R. L. Edwards, H. Cheng, and C. D. Charles, 2020: No consistent ENSO response to volcanic forcing over the last millennium. *Science*, **367**, 1477–1481, <https://doi.org/10.1126/science.aax2000>.
- Deser, C., and Coauthors, 2012: ENSO and Pacific decadal variability in the Community Climate System Model version 4. *J. Climate*, **25**, 2622–2651, <https://doi.org/10.1175/JCLI-D-11-00301.1>.
- Dewitte, B., 2000: Sensitivity of an intermediate ocean–atmosphere coupled model of the tropical Pacific to its oceanic vertical structure. *J. Climate*, **13**, 2363–2388, [https://doi.org/10.1175/1520-0442\(2000\)013<2363:SOAIOA>2.0.CO;2](https://doi.org/10.1175/1520-0442(2000)013<2363:SOAIOA>2.0.CO;2).

- , S. Thual, S. W. Yeh, S. I. An, B. K. Moon, and B. S. Giese, 2009: Low-frequency variability of temperature in the vicinity of the equatorial Pacific thermocline in SODA: Role of equatorial wave dynamics and ENSO asymmetry. *J. Climate*, **22**, 5783–5795, <https://doi.org/10.1175/2009JCLI2764.1>.
- DiNezio, P. N., and J. E. Tierney, 2013: The effect of sea level on glacial Indo-Pacific climate. *Nat. Geosci.*, **6**, 485–491, <https://doi.org/10.1038/ngeo1823>.
- , G. A. Vecchi, and A. C. Clement, 2013: Detectability of changes in the Walker circulation in response to global warming. *J. Climate*, **26**, 4038–4048, <https://doi.org/10.1175/JCLI-D-12-00531.1>.
- Fedorov, A. V., and S. G. Philander, 2001: A stability analysis of tropical ocean-atmosphere interactions: Bridging measurements and theory for El Niño. *J. Climate*, **14**, 3086–3101, [https://doi.org/10.1175/1520-0442\(2001\)014<3086:ASAOTO>2.0.CO;2](https://doi.org/10.1175/1520-0442(2001)014<3086:ASAOTO>2.0.CO;2).
- Ferrett, S., M. Collins, and H.-L. Ren, 2018: Diagnosing relationships between mean state biases and El Niño shortwave feedback in CMIP5 models. *J. Climate*, **31**, 1315–1335, <https://doi.org/10.1175/JCLI-D-17-0331.1>.
- Ford, H. L., A. C. Ravelo, and P. J. Polissar, 2015: Reduced El Niño–Southern Oscillation during the Last Glacial Maximum. *Science*, **347**, 255–258, <https://doi.org/10.1126/science.1258437>.
- Gao, C., A. Robock, and C. Ammann, 2008: Volcanic forcing of climate over the past 1500 years: An improved ice core-based index for climate models. *J. Geophys. Res.*, **113**, D23111, <https://doi.org/10.1029/2008JD010239>.
- Haslett, J., and A. Parnell, 2008: A simple monotone process with application to radiocarbon-dated depth chronologies. *J. Roy. Stat. Soc.*, **57C**, 399–418, <https://doi.org/10.1111/j.1467-9876.2008.00623.x>.
- Hayashi, M., and F. F. Jin, 2017: Subsurface nonlinear dynamical heating and ENSO asymmetry. *Geophys. Res. Lett.*, **44**, 12 427–12 435, <https://doi.org/10.1002/2017GL075771>.
- Higley, M. C., J. L. Conroy, and S. Schmitt, 2018: Last millennium meridional shifts in hydroclimate in the central tropical Pacific. *Paleoceanogr. Paleoclimatol.*, **33**, 354–366, <https://doi.org/10.1130/ABS/2018AM-320093>.
- Huang, B., and Coauthors, 2017: NOAA Extended Reconstructed Sea Surface Temperature (ERSST), version 5. NOAA National Centers for Environmental Information, accessed 11 July 19, <https://doi.org/10.7289/V5T72FNM>.
- Jin, F.-F., S.-I. An, A. Timmermann, and J. X. Zhao, 2003: Strong El Niño events and nonlinear dynamical heating. *Geophys. Res. Lett.*, **30**, 1120, <https://doi.org/10.1029/2002GL016356>.
- Karamperidou, C., M. A. Cane, U. Lall, and A. T. Wittenberg, 2014: Intrinsic modulation of ENSO predictability viewed through a local Lyapunov lens. *Climate Dyn.*, **42**, 253–270, <https://doi.org/10.1007/s00382-013-1759-z>.
- , P. N. Di Nezio, A. Timmermann, F. F. Jin, and K. M. Cobb, 2015: The response of ENSO flavors to mid-Holocene climate: Implications for proxy interpretation. *Paleoceanography*, **30**, 527–547, <https://doi.org/10.1002/2014PA002742>.
- , F. F. Jin, and J. L. Conroy, 2017: The importance of ENSO nonlinearities in tropical Pacific response to external forcing. *Climate Dyn.*, **49**, 2695–2704, <https://doi.org/10.1007/s00382-016-3475-y>.
- Karnauskas, K. B., J. E. Smerdon, R. Seager, and J. F. González-Rouco, 2012: A Pacific centennial oscillation predicted by coupled GCMs. *J. Climate*, **25**, 5943–5961, <https://doi.org/10.1175/JCLI-D-11-00421.1>.
- Koutavas, A., and S. Ioannides, 2012: El Niño–Southern Oscillation extrema in the Holocene and Last Glacial Maximum. *Paleoceanography*, **27**, PA4208, <https://doi.org/10.1029/2012PA002378>.
- Li, J., S.-P. Xie, E. R. Cook, G. Huang, R. D’Arrigo, F. Liu, J. Ma, and X.-T. Zheng, 2011: Interdecadal modulation of El Niño amplitude during the past millennium. *Nat. Climate Change*, **1**, 114–118, <https://doi.org/10.1038/nclimate1086>.
- Liang, J., X.-Q. Yang, and D. Z. Sun, 2012: The effect of ENSO events on the tropical Pacific mean climate: Insights from an analytical model. *J. Climate*, **25**, 7590–7606, <https://doi.org/10.1175/JCLI-D-11-00490.1>.
- Masson-Delmotte, V., and Coauthors, 2013: Information from paleoclimate archives. *Climate Change 2013: The Physical Science Basis*, T. F. Stocker et al., Eds., Cambridge University Press, 383–464.
- Meehl, G. A., C. Covey, T. Delworth, M. Latif, B. McAvaney, J. F. B. Mitchell, R. J. Stouffer, and K. E. Taylor, 2007: The WCRP CMIP3 multimodel dataset: A new era in climate change research. *Bull. Amer. Meteor. Soc.*, **88**, 1383–1394, <https://doi.org/10.1175/BAMS-88-9-1383>.
- Oster, J. L., D. E. Ibarra, M. J. Winnick, and K. Maher, 2015: Steering of westerly storms over western North America at the Last Glacial Maximum. *Nat. Geosci.*, **8**, 201–205, <https://doi.org/10.1038/ngeo2365>.
- Pausata, F. S. R., C. Karamperidou, R. Caballero, and D. S. Battisti, 2016: ENSO response to high-latitude volcanic eruptions in the Northern Hemisphere: The role of the initial conditions. *Geophys. Res. Lett.*, **43**, 8694–8702, <https://doi.org/10.1002/2016GL069575>.
- , D. Zanchettin, C. Karamperidou, R. Caballero, and D. S. Battisti, 2020: ITCZ shift and extra-tropical teleconnections drive ENSO response to volcanic eruptions. *Sci. Adv.*, **6**, eaaz5006, <https://doi.org/10.1126/sciadv.aaz5006>.
- Rayner, N. A., D. E. Parker, E. B. Horton, C. K. Folland, L. V. Alexander, D. P. Rowell, E. C. Kent, and A. Kaplan, 2003: Global analyses of sea surface temperature, sea ice, and night marine air temperature since the late nineteenth century. *J. Geophys. Res.*, **108**, 4407, <https://doi.org/10.1029/2002JD002670>.
- Roberts, W. H. G., D. S. Battisti, and A. W. Tudhope, 2014: ENSO in the mid-Holocene according to CSM and HadCM3. *J. Climate*, **27**, 1223–1242, <https://doi.org/10.1175/JCLI-D-13-00251.1>.
- Rodionov, S. N., 2004: A sequential algorithm for testing climate regime shifts. *Geophys. Res. Lett.*, **31**, L09204, <https://doi.org/10.1029/2004GL019448>.
- , 2006: Use of prewhitening in climate regime shift detection. *Geophys. Res. Lett.*, **33**, L12707, <https://doi.org/10.1029/2006GL025904>.
- Rustic, G. T., A. Koutavas, T. M. Marchitto, and B. K. Linsley, 2015: Dynamical excitation of the tropical Pacific Ocean and ENSO variability by Little Ice Age cooling. *Science*, **350**, 1537–1541, <https://doi.org/10.1126/science.aac9937>.
- Sadekov, A. Y., R. Ganeshram, L. Pichevin, R. Berdin, E. McClymont, H. Elderfield, and A. W. Tudhope, 2013: Palaeoclimate reconstructions reveal a strong link between El Niño–Southern Oscillation and tropical Pacific mean state. *Nat. Commun.*, **4**, 2692, <https://doi.org/10.1038/ncomms3692>.
- Samanta, D., K. B. Karnauskas, N. F. Goodkin, S. Coats, J. E. Smerdon, and L. Zhang, 2018: Coupled model biases breed spurious low-frequency variability in the tropical Pacific Ocean. *Geophys. Res. Lett.*, **45**, 10 609–10 618, <https://doi.org/10.1029/2018GL079455>.
- Schmidt, G. A., and Coauthors, 2011: Climate forcing reconstructions for use in PMIP simulations of the last millennium (v1.0). *Geosci. Model Dev.*, **4**, 33–45, <https://doi.org/10.5194/gmd-4-33-2011>.
- , and Coauthors, 2012: Climate forcing reconstructions for use in PMIP simulations of the Last Millennium (v1.1). *Geosci. Model Dev.*, **5**, 185–191, <https://doi.org/10.5194/gmd-5-185-2012>.
- , and Coauthors, 2013: Using paleo-climate comparisons to constrain future projections in CMIP5. *Climate Past Discuss.*, **9**, 775–835, <https://doi.org/10.5194/cpd-9-775-2013>.

- Seager, R., M. Cane, N. Henderson, D. E. Lee, R. Abernathey, and H. Zhang, 2019: Strengthening tropical Pacific zonal sea surface temperature gradient consistent with rising greenhouse gases. *Nat. Climate Change*, **9**, 517–522, <https://doi.org/10.1038/s41558-019-0505-x>.
- Stevenson, S., B. Otto-Bliesner, J. Fasullo, and E. Brady, 2016: “El Niño like” hydroclimate responses to last millennium volcanic eruptions. *J. Climate*, **29**, 2907–2921, <https://doi.org/10.1175/JCLI-D-15-0239.1>.
- Sun, D. Z., 2003: A possible effect of an increase in the warm-pool SST on the magnitude of El Niño warming. *J. Climate*, **16**, 185–205, [https://doi.org/10.1175/1520-0442\(2003\)016<0185:APEOAI>2.0.CO;2](https://doi.org/10.1175/1520-0442(2003)016<0185:APEOAI>2.0.CO;2).
- Timmermann, A., 2003: Decadal ENSO amplitude modulations: A nonlinear paradigm. *Global Planet. Change*, **37**, 135–156, [https://doi.org/10.1016/S0921-8181\(02\)00194-7](https://doi.org/10.1016/S0921-8181(02)00194-7).
- , and F. F. Jin, 2002: A nonlinear mechanism for decadal El Niño amplitude changes. *Geophys. Res. Lett.*, **29**, 1003, <https://doi.org/10.1029/2001GL013369>.
- Vecchi, G., A. Clement, B. J. Soden, 2008: Examining the tropical Pacific’s response to global warming. *Eos, Trans. Amer. Geophys. Union*, **89**, 81–83, <https://doi.org/10.1029/2008EO090002>.
- Watanabe, S., and Coauthors, 2011: MIROC-ESM 2010: Model description and basic results of CMIP5-20c3m experiments. *Geosci. Model Dev.*, **4**, 845–872, <https://doi.org/10.5194/gmd-4-845-2011>.
- Wittenberg, A. T., 2002: ENSO response to altered climates. Ph.D. thesis, Princeton University, 475 pp., <https://doi.org/10.13140/RG.2.1.1777.8403>.
- , 2009: Are historical records sufficient to constrain ENSO simulations? *Geophys. Res. Lett.*, **36**, L12702, <https://doi.org/10.1029/2009GL038710>.
- Yeh, S.-W., and B. P. Kirtman, 2004: Tropical Pacific decadal variability and ENSO amplitude modulation in a CGCM. *J. Geophys. Res.*, **109**, C11009, <https://doi.org/10.1029/2004JC002442>.
- Zebiak, S. E., and M. A. Cane, 1987: A model El Niño–Southern Oscillation. *Mon. Wea. Rev.*, **115**, 2262–2278, [https://doi.org/10.1175/1520-0493\(1987\)115<2262:AMENO>2.0.CO;2](https://doi.org/10.1175/1520-0493(1987)115<2262:AMENO>2.0.CO;2).
- Zhao, M., C. Y. Huang, C. C. Wang, and G. Wei, 2006: A millennial-scale U37K’ sea-surface temperature record from the South China Sea (8°N) over the last 150 kyr: Monsoon and sea-level influence. *Palaeogeogr. Palaeoclimatol. Palaeoecol.*, **236**, 39–55, <https://doi.org/10.1016/j.palaeo.2005.11.033>.